ADVANCED MATERIALS INTERFACES
Open Access
www.advmatinterfaces.de

Unraveling Enyne Bonding via Dehydrogenation–Hydrogenation Processes in On-Surface Synthesis with Terminal Alkynes

Yuanhao Lyu, Feng Gao, Peng Cheng, Lan Chen, Svetlana Klyatskaya, Mario Ruben, Johanna Rosen, Johannes V. Barth, Jonas Björk, Kehui Wu,* and Yi-Qi Zhang**

On-surface reactions of terminal alkynes in ultrahigh vacuum have attracted widespread attention due to their high technological promise. However, employing different precursors and substrate materials often intricate reaction schemes appear far from being well-understood. Thus, recent investigations of alkyne coupling on noble metal surfaces suggest non-dehydrogenative scenarios, contradicting earlier reports. Herein, the study employs noncontact atomic force microscopy (nc-AFM) with high spatial resolution to conclusively characterize exemplary alkyne coupling products. Contrary to initial interpretations proposing dehydrogenative homocoupling on Ag(111), bond-resolved AFM imaging reveals the expression of enyne motifs. Based on complementary, extensive density functional theory calculations, the pertaining reaction mechanisms are explored. It is proposed that enyne formation initiates with a direct carbon–carbon coupling between two alkyne groups, followed by surface-assisted dehydrogenation-hydrogenation processes. Thereby consecutive steps of atomic hydrogen cleavage, surface migration and recombination to a different carbon atom enable bridging via carbon–carbon double bonding. The new results shed light on subtle, but crucial surface-mediated hydrogen transfer processes involved in the chemical bond formation, which are suggested to be of general relevance in on-surface synthesis.

1. Introduction

The highly promising research domain of interfacial synthesis with adsorbed organic precursors under ultrahigh vacuum (UHV) conditions opens new avenues toward atomically precise fabrication of synthetic low-dimensional covalent architectures with designed properties.[1] In this context, on-surface reactions of terminal alkynes were extensively explored,[2] largely motivated by the associated prospects for realizing low-dimensional materials and nanostructures containing sp- and sp^2-hybridized carbons, notably including the appealing two-dimensional (2D) materials such as graphyne (GY) and graphdiyne (GDY).[3] Although achieving pure covalent crystalline single sheets of GY and GDY remains challenging, a remarkable variety of on-surface reaction schemes with terminal alkynes have been unveiled.[4] Exemplary protocols include homocoupling,[2a,b,5]

Y. Lyu, F. Gao, P. Cheng, L. Chen, K. Wu, Y.-Q. Zhang
Institute of Physics
Chinese Academy of Sciences
Beijing 100190, China
E-mail: khwu@iphy.ac.cn; yiqi.zhang@iphy.ac.cn
Y. Lyu, F. Gao, P. Cheng, L. Chen, K. Wu
School of Physical Sciences
University of Chinese Academy of Sciences
Beijing 100190, China

The ORCID identification number(s) for the author(s) of this article can be found under https://doi.org/10.1002/admi.202400222

DOI: 10.1002/admi.202400222

L. Chen, K. Wu
Songshan Lake Materials Laboratory
Dongguan, Guangdong 523808, China
S. Klyatskaya, M. Ruben
Institute of Nanotechnology
Karlsruhe Institute of Technology (KIT)
D-76344 Eggenstein-Leopoldshafen, Germany
M. Ruben
IPCMS-CNRS
Université de Strasbourg
Strasbourg F-67034, France
J. Rosen, J. Björk
Department of Physics, Chemistry and Biology (IFM)
Linköping University
Linköping SE-58183, Sweden
E-mail: jonas.bjork@liu.se
J. V. Barth
Physics Department E20
Technical University of Munich
D-85748 Garching, Germany

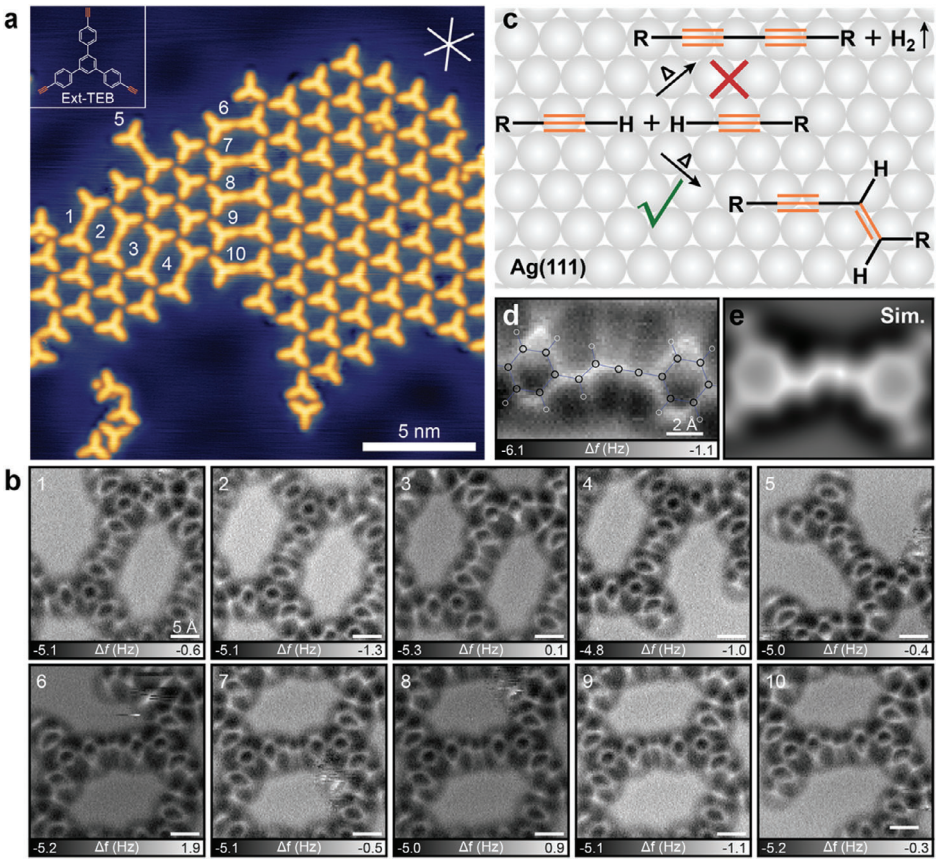

Figure 1. Ext-TEB molecular island on Ag(111) after annealing at 350 K. a) STM image showing the molecular island of coexisting covalent dimer and intact monomers. (U_b = 20 mV, I_t = 5 pA, T_{STM} = 4.8 K, with a CO-terminated tip). Inset: chemical structure of the Ext-TEB molecule. b) Filtered AFM images showing ten Ext-TEB dimers in (a). c) Two possible alkyne coupling pathways result in butadiyne and enyne linkages, respectively. On Ag(111), enyne formation is favored. d) Zoomed-in AFM image of the enyne connection with a structural model superimposed. e) DFT-simulated AFM image of a TEB dimer, featuring an enyne bridge.

Sonogashira-type cross coupling,[6] cyclotrimerization,[2c,7] cycloaddition,[8] and cyclization reactions.[9] For molecular precursors comprising terminal alkyne and aryl halide moieties, in addition intricate reaction pathways yielding organometallic complexes were introduced.[10] More recently, proton-tunneling-mediated molecular conversion as well as gas-mediated dehydrogenation processes well below room temperatures were exploited, featuring high chemoselectivity.[11]

It is noteworthy that several research groups recently deduced non-dehydrogenative coupling between terminal alkynes on noble metal surfaces,[9b,12] whereas dehydrogenative alkyne coupling takes place on Au(111) for alkyne derivatives with either halogen-substitution or a pyridine backbone.[5,12b] These new results imply an underlying reaction pathway fundamentally different from the classical Glaser-Hay coupling,[13] while contradicting initial conclusions drawn from scanning tunneling microscopy (STM) and density functional theory (DFT) modeling claiming that homocoupling between terminal alkynes entails formation of a butadiyne (diacetylene) linkage on Ag(111) (cf. reaction scheme in **Figure 1c**).[2a,b] To establish a coherent understanding of homocoupling reaction pathways on noble metal surfaces,[13c] it is important to employ advanced high-resolution imaging techniques.[14]

In this study, we carried out experiments in a combined scanning tunneling and non-contact atomic force microscopy (STM/AFM) system equipped with a qPlus sensor.[15] Using carbon monoxide (CO) functionalized tips, we were able to resolve and identify the chemical nature of the covalent bonds formed via alkyne coupling on Ag(111) at different temperatures. We found that at 350 K, the terminal alkynes favor enyne-bridge formation with a high chemoselectivity rather than forming the 1,3-butadiyne bridge. After 400 K annealing, nanoporous polymeric structures were formed with dominating enyne connections. Through comprehensive DFT modeling, we unravel a novel mechanism for the enyne formation, which is initiated by a similar direct linking between two terminal alkynes but is followed by a distinct dehydrogenation-hydrogenation process with a lower activation energy. More specifically, the split-off hydrogen preferentially migrates on the surface to recombine with the unsaturated carbon, resulting in the formation of a C—C double bond. In comparison, the associative desorption pathway, involving recombination with another hydrogen adatom, is less favored as it requires a higher activation energy. Interestingly, DFT-predicted reaction intermediates evolving in the dehydrogenation process, were captured in the experiments. The presence of these uncompleted enyne bridges implies that the split-off hydrogen

could also engage in the associative desorption process. Our results provide deep insight into surface-assisted hydrogen-transfer processes involved in the chemical bond formation.

2. Results and Discussion

In this study, we utilized the same molecular precursor, 1,3,5- tris-(4-ethynylphenyl)benzene (Ext-TEB), as in our original work.[2a] Ext-TEB molecules were deposited onto the Ag(111) substrate held at room temperature, leading to the formation of highly regular supramolecular domains of densely-packed molecules (Figure S1, Supporting Information).[16] Upon annealing the substrate to 350 K, the emergence of covalent dimers alongside unreacted Ext-TEB species is observed (Figure 1a), being consistent with our earlier study.[2a] Here, a CO-functionalized tip is used for STM imaging under the constant-current mode (Figure 1a). Although the image resolution is enhanced in comparison to using a bare W-tip (Figure S2, Supporting Information), the covalent bridges of the dimers embedded in the island appear straight, and no further details of their chemical structures can be extracted. In our previous work, based on STM imaging, X-ray photoelectron spectroscopy and DFT calculations, we concluded that the homocoupling of two terminal alkynes leads to the formation of 1,3-butadiyne bridge[2a,13c] (cf. reaction path in the upper panel of Figure 1c).

To elucidate the chemical nature of the covalent bond, we switched to the AFM mode and recorded frequency shift (Δf) images using the same CO-tip under the constant-height mode.[14a,b] Figure 1b depicts ten dimers with chemical bond resolution. Each half of the dimer is clearly identified as consisting of four phenyl rings. The central ring appears symmetric, whereas three outer phenyl rings appear elongated (cf. also Figure S3, Supporting Information),[17] a feature attributed to the lateral deflections of the terminal CO molecule.[18] Surprisingly, upon scrutinizing all ten dimers within the island (Figure 1a,b), it becomes evident that the covalent bridge is kinked, deviating from the anticipated linear butadiyne linkage.[5] Instead, these kinked covalent connections are more likely associated with the enyne bridges[12b,c] (cf. also Figures S3 and S4, Supporting Information). Figure 1d displays a magnified covalent connection superimposed with a structural model of the enyne bridge. It can be seen that the bright protrusion in the AFM image corresponds to the C–C triple bond, in accordance with observations reported in the literature.[9b,19] Notably, the kink in the covalent connection, which becomes prominent at smaller tip-sample distances (Figure S3, Supporting Information), is attributed to the C–C double bond. Discrimination of C—C bond order requires site-specific force-distance spectroscopic characterization,[14b,15a] which calls for further investigations. Figure 1e depicts a DFT-simulated AFM image of an enyne bridge based on a 1,3,5-triethynyl-benzene (TEB) dimer (cf. **S4** in Figure 4b). Both the bright protrusion (C–C triple bond) and the kink (C–C double bond) in the enyne linkage are well reproduced. However, the deformation of the outer-phenyl-ring in the AFM image due to CO tilt is not captured. This discrepancy could be attributed to the employed TEB-dimer model, wherein two hydrogen atoms on each phenyl ring (Figure 1d) are substituted by terminal alkynes.[20] To further corroborate this finding, we examined 43 dimers in several Ext-TEB molecular islands through bond-resolved AFM imaging, consistently confirming the absence of dehydrogenated terminal alkyne homocoupling products.

After annealing the sample at 400 K, the formation of open porous networks was observed (Figure S5, Supporting Information), consistent with our earlier report.[2a] **Figure 2** illustrates one of the six-membered polymeric rings formed through the coupling of Ext-TEB molecules, initially ascribed to graphdiyne-like scaffolds.[2a] However, the high-resolution AFM image reveals that each covalent bridge is not linear but adopts an enyne-like structure (cf. Figure 2b,c), suggesting that the non-dehydrogenative coupling remains dominating after 400 K annealing.

Figure 3 displays the statistical analysis of 55 dimers within the polymeric networks. The annealing at 400K results in the formation of various types of covalent connections, with enyne bridges being predominant. Occasionally, butadiyne linkages can also be observed (Figure 3a). The observed butadiyne connection shown in Figure 3a is slightly bent as a result of the adsorption configurations of Ext-TEB molecules on either side of the covalent dimer (Figure S6, Supporting Information). Trans and cis forms of enyne bridges (Figure 3b–d) are the major products after 400 K annealing. Trans-enyne-bridges were commonly observed with slight bending (Figure 3b), whereas in some cases, strongly bent geometries were found (Figure 3c), mainly due to the strain introduced by adsorption configurations on both sides of the dimer (Figure S7, Supporting Information). Additionally, rare butadiene bridges were also observed (Figure 3e), indicating the uptake of two additional hydrogen atoms from the substrate during covalent bond formation. In Figure 3f, a previously unreported covalent connection is depicted. This particular structural motif exhibits a kink of ≈90-degree, as indicated by an arrow in Figure 3fiii. Notably, at this kinked node, no apparent bond length is discernible. Instead, it features a distinct point, which is markedly different from the C–C double bond present in the cis-enyne-bridge (cf. Figure 3diii). We assign this connection to a putative "uncompleted" enyne bridge that lacks a hydrogen atom and therefore has a carbon radical site (denote as sp^2-hybridized carbon-centered enyne radical; Figure 3fiii; Figure S8, Supporting Information). This could be viewed as the intermediate structure that supports the DFT modeling of the enyne formation pathway, which will be discussed in detail below. Additionally, some cases of a strained enyne radical structure were observed (Figure 3g).

In addition, coupling motifs connecting three Ext-TEB molecules were also examined (Figure S9, Supporting Information). Previously, we proposed that such nodes can be interpreted as enediyne motifs resulting from a butadiyne bridge being attacked by a terminal alkyne group.[21] With bond-resolved AFM imaging, this branched structure is revealed to contain a 1,3-butadiene-like moiety, which is consistent with the addition of another alkyne group to an enyne bridge (Figure S9, Supporting Information). Therefore, our current results indicate that coupling of three terminal alkynes is also non-dehydrogenative.

To better understand the enyne formation mechanism, extensive DFT simulations were carried out. From our previous study, it was demonstrated that the coupling between two intact molecules is significantly more favorable than both the dehydrogenation and tautomerization of a single molecule,[13c] which harmonizes with a reaction where no hydrogen abstraction has taken

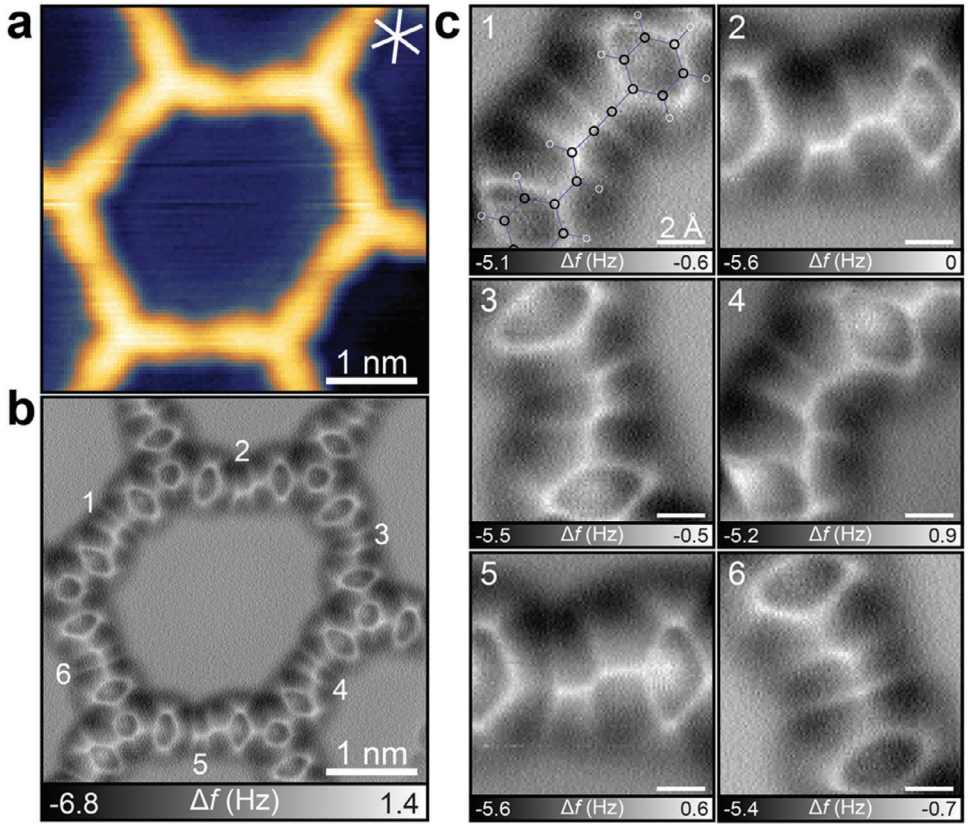

Figure 2. Formation of a six-membered polymeric ring composed of Ext-TEB on Ag(111) after annealing at 400 K. a) STM image of the six-membered ring. (U_b = 20 mV, I_t = 5 pA, T_{STM} = 4.8 K, with a CO tip). b) Filtered AFM image showing bond-resolved structure in (a). c) Zoomed-in AFM images (with filtering) of each covalent bond formed between Ext-TEB molecules. A scaled structural model is superimposed on (c–1).

place. The coupling can either result in two different conformations, with either one or two C—Ag bonds, where the latter is more favorable. Beginning with the coupled dimer, two subsequent C—H activations lead to the butadiyne bridge, while the enyne formation requires hydrogen transfer reactions. Both reactions require the simultaneous breaking of the C—Ag bonds.

With the initially coupled dimer as starting point in its most stable conformation with two C—Ag bonds, we first examined enyne formation through tautomerization steps (Figures S10 and S11, Supporting Information). However, the tautomerization reactions are associated with significantly larger activation energies than that for butadiyne formation and can thus be disregarded. We also explored alternative scenarios where Ag adatoms participate during the tautomerization yet found that they do not aid the enyne formation (Figures S12–S17, Supporting Information).

Instead, we found a process, in which the initial coupling is followed by dehydrogenation and the concomitant reattachment of the hydrogen to another carbon to form the enyne motif, being significantly more favorable than other considered pathways. The complete pathway, from individual monomers to the enyne-connected dimer, is depicted in **Figure 4**. The first three steps (**S0** to **S3**) are the same as for the butadiyne formation.[13c] The two monomers couple (**S0** to **S1**) with an activation free energy of 0.89 eV, followed by a conformational transformation involving the breaking of a C—Ag bond (**S1** to **S2**) and subsequent dehydrogenation (**S2** to **S3**). The effective activation free energy from **S1** to **S3** is determined by the free energy difference between **TS2** and **S1** (1.12 eV). The transition from **S3** to **S4** involves a surface-mediated hydrogenation process: the split-off hydrogen atom first migrates on the surface and subsequently recombines with the unsaturated alkyne carbon atom on the other half of the TEB dimer. Note that this carbon atom is bonded toward the substrate (**S3** in Figure 4), and its hydrogenation simultaneously breaks the C—Ag bond, completing the enyne formation process. Notably, the activation energy for this hydrogenation step (**S3** to **S4**) is merely 0.51 eV. Once reaching **S4** the free energy is significantly reduced, and thus this final step of the reaction can be considered as irreversible at the temperature of the reaction.

To corroborate the hydrogenation process from **S3** to **S4**, we need to ensure that the competing process of the associative desorption of hydrogen, which is often observed as a consequence of dehydrogenation reactions,[22] is unfavorable. Notably, through further DFT calculations, the activation free energy of this process is found to be 0.68 eV (Figure S18, Supporting Information). Given a temperature of 350 K, the hydrogenation process has a Boltzmann factor more than two orders of magnitude times that of the associative desorption of hydrogen. In other words, the enyne formation will dominate over the hydrogen desorption, providing further support for the presented pathway. It is noteworthy that the experimental data from 400 K annealing unveils reaction products which can be interpreted as "trapped

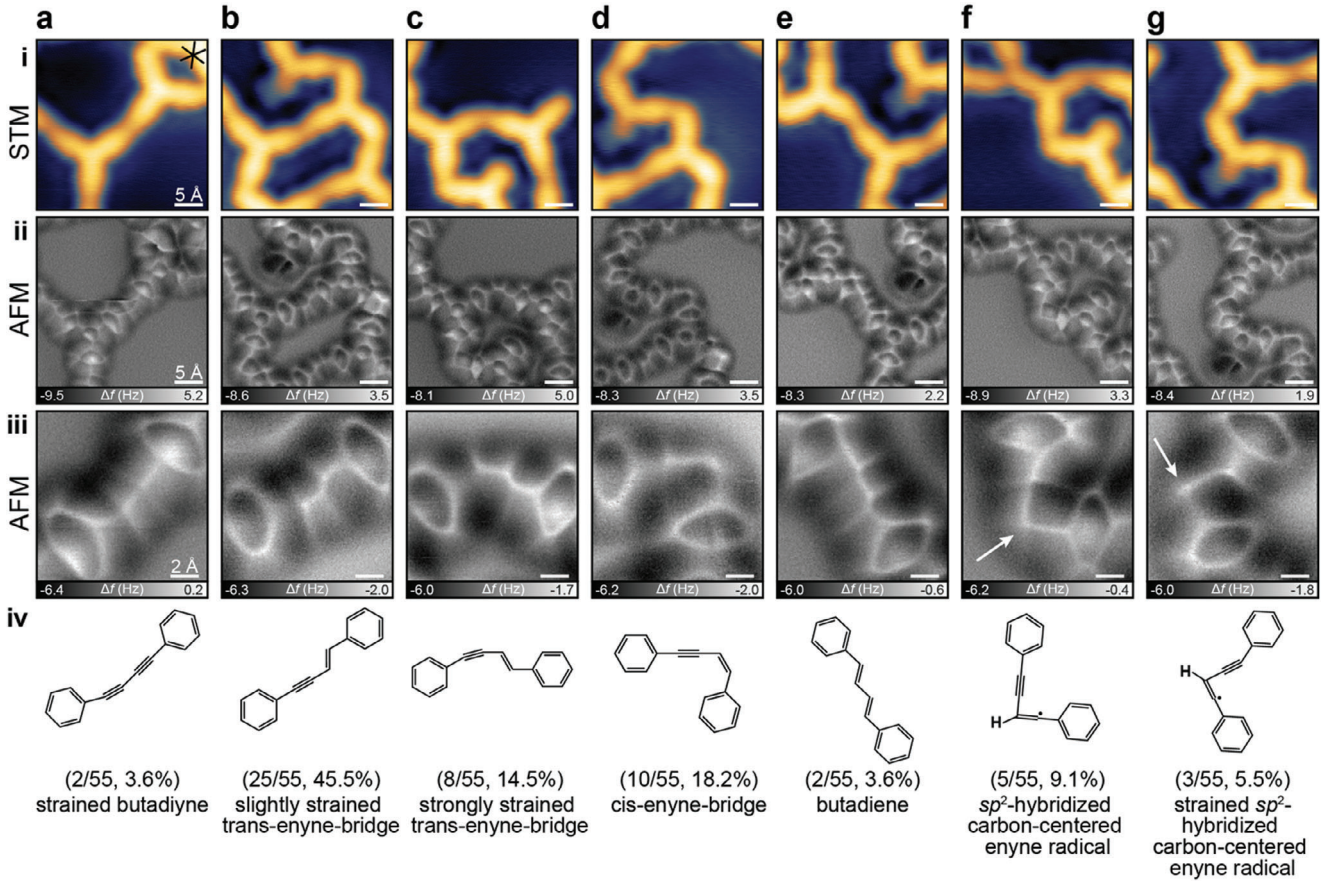

Figure 3. Identification of various types of products after annealing at 400 K. a–g) Typical covalent connections formed after 400 K annealing. i) STM images (U_b = 20 mV, I_t = 5 pA, T_{STM} = 4.8 K, with a CO tip); ii) Corresponding filtered AFM images; iii) Magnified covalent bridges in (ii); iv) Chemical structures with statistical distributions. A total of 55 covalent bridges were analyzed.

intermediates", namely, the "uncompleted" enyne bridge with one hydrogen atom missing (Figure 3f,g; Figure S8, Supporting Information). These structures with a yield of ≈15% not only support the dehydrogenation-hydrogenation pathway, but also provide evidence of associative desorption of hydrogen on the surface.

Finally, it should be noted that the values reported in the pathway in Figure 4 for **S0**-**S3** differ slightly from the corresponding values in our original report.[13c] This is mainly due to the inclusion of finite temperature effects in the present study, but also affected by a slightly different exchange-correlation functional and a more rigid *k*-point sampling applied. In the Supporting Information (Figure S19, Supporting Information) the potential energy pathway at 0 K is shown to enable a direct comparison.

3. Conclusion

The homocoupling between terminal alkyne species on Ag(111) under mild condition was closely examined by means of bond-resolved AFM imaging. We can safely conclude that enyne bonding prevails at 350 K with high chemoselectivity, rather than previously reported butadiyne formations. Furthermore, after 400 K annealing, we observed the emergence of several types of products, including butadiyne, butadiene, and possible enyne radicals. Nonetheless, enyne bridges remain predominant, while dehydrogenative coupling is rarely observed. Comprehensive DFT modeling unveils a distinct dehydrogenation–hydrogenation process mediated via hydrogen adatom migration, facilitating the enyne formation. Our computational analysis provides the first mechanistic insight into surface-assisted hydrogen transfer process, playing a decisive role in the chemical bond formation. Similar on-surface hydrogen transfer processes have been invoked for other types of on-surface reactions,[10c,12b,23] although the detailed mechanisms remain to be disentangled. Our current results not only contribute to a coherent understanding of on-surface reaction mechanisms associated with alkyne derivatives but also highlight the important role played by surface-mediated hydrogen migration and transfer processes in the formation and steering of chemical bonds in on-surface synthesis.

4. Experimental Section

The clean Ag(111)/mica surfaces were prepared by repeated cycles of Ar^+ sputtering and annealing to 670 K. Molecules were sublimated by organic molecular epitaxy from a quartz crucible at $T_{crucible} \approx 365$K. Ext-TEB molecules were dosed onto the clean Ag(111) surface held at

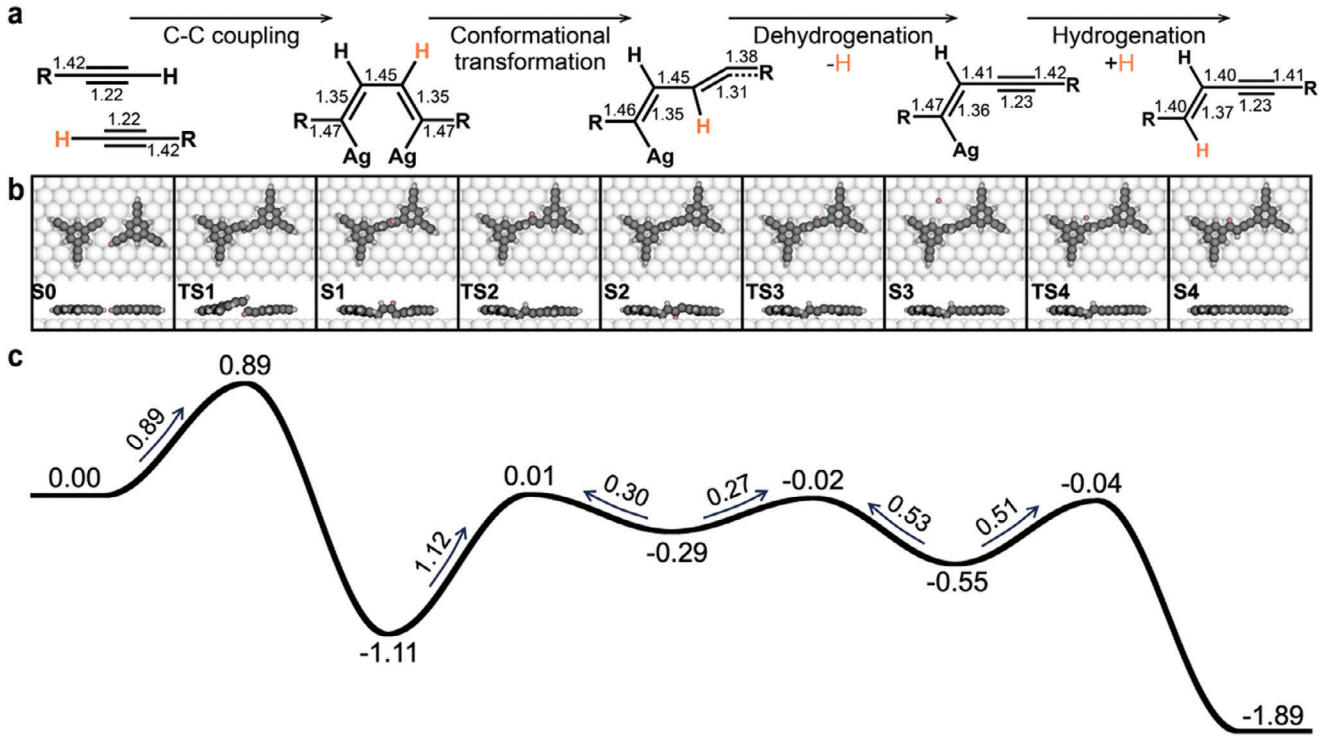

Figure 4. Calculated reaction pathway for the enyne formation with a) valence bond structures of local minima (**S0**–**S4**) together with b) top and side views of local minima and transition states (**TS1**–**TS4**) and corresponding free energy profile at 350 K (c). In (a), bond lengths of the relevant carbon–carbon bonds are indicated. The hydrogen atom involved in the subsequent dehydrogenation and hydrogenation processes is rendered in pink throughout the reaction. Bond lengths are given in Å and energies in eV.

300 K, and subsequent annealing to 350 and 400 K was performed to facilitate molecular reactions. The STM/AFM measurements were carried out in a Polar STM/AFM system (Scienta Omicron) at 4.8 K with base pressure $< 2 \times 10^{-10}$ mbar. The used qPlus sensor had a resonance frequency $f_0 = 24.5$ kHz, a spring constant $k_0 \approx 1800$ N m^{-1}, and a quality factor of $Q \approx 170000$ at 4.8 K. Oscillation amplitudes A = 0.5 Å were used. All STM and AFM images were recorded in constant-current, and constant-height modes, respectively, with a CO-terminated tip.

Periodic DFT calculations were done with the VASP code,[24] employing the projector augmented wave method[25] to describe core electrons and a plane wave basis set expanded to a kinetic energy cutoff of 400 eV. Exchange-correlation effects were described by the van der Waals density functional[26] with the version by Hamada denoted as rev-vdWDF2,[27] which has shown to describe the adsorption of organic molecules on coinage metals accurately.[28] The Ag(111) surface was represented by a four-layered slab. For all calculations, a p(10 × 9) surface unit cell together was used with a 3 × 3 *k*-point sampling, ensuring a numerical convergence within 10 meV of all reported values. Transition states were found using a combination of the Climbing Image Nudge Elastic Band (CI-NEB)[29] and Dimer methods,[30] where CI-NEB was used to provide an initial guess of a transition state to be refined by the Dimer method. All structures (local minima as well as transition states) were geometrically optimized until the residual forces on all atoms (except the two bottom layers of the Ag(111) slab which were kept fixed) were <0.01 eV Å^{-1}. Free energies were evaluated by adding vibrational enthalpy and entropy to the DFT energies, using vibrational energies obtained within the framework of the harmonic approximation, with derivatives of forces calculated by finite differences. In evaluation of vibrational energies, we only considered the atoms of the two terminal alkynes taking part in the coupling and the Ag atoms of the outmost surface layer interacting chemically with the terminal alkynes. AFM simulations were done with the probe-particle model,[18c,31] using a CO molecule as probe. Pauli repulsion and van der Waals interactions were modeled by Lennard-Jones potentials while electrostatic interactions were included using the Hartree potential obtained from DFT and with a quadrupole representing the CO. The probe was restrained in the xy-plane by a harmonic spring with a stiffness of 0.24 N m^{-1}.

Supporting Information

Supporting Information is available from the Wiley Online Library or from the author.

Acknowledgements

This work was financially supported by the National Natural Science Foundation of China (12174431 and 1192780039) and the Strategic Priority Research Program of the Chinese Academy of Sciences (XDB30000000). J.B. and J.R. acknowledge financial support by the Swedish Research Council and the Swedish Government Strategic Research Area in Materials Science on Functional Materials at Linköping University (Faculty Grant SFO-Mat-LiU no. 2009-00971). The computations were enabled by resources provided by the National Academic Infrastructure for Supercomputing in Sweden (NAISS) at PDC Center for High Performance Computing, partially funded by the Swedish Research Council through grant agreements no. 2022-06725. S.K. and M.R. acknowledge funding by the German Research Foundation (DFG) through the priority programs 1928 COORNETs and European Union's Framework Programme for Research and Innovation, Horizon 2020, under the Marie Sklodowska-Curie Grant Agreement No. 847471 (QUSTEC). J.V.B. acknowledges support from the Munich Quantum Center, and the DFG Excellence Cluster e-conversion.

Conflict of Interest

The authors declare no conflict of interest.

Data Availability Statement

The data that support the findings of this study are available from the corresponding author upon reasonable request.

Keywords

density functional theory, graphdiyne, non-contact atomic force microscopy, on-surface synthesis, terminal alkyne

Received: March 27, 2024
Published online: April 15, 2024

[1] a) L. Grill, M. Dyer, L. Lafferentz, M. Persson, M. V. Peters, S. Hecht, *Nat. Nanotechnol.* **2007**, *2*, 687; b) P. A. Held, H. Fuchs, A. Studer, *Chem.-Eur. J.* **2017**, *23*, 5874; c) S. Clair, D. G. de Oteyza, *Chem. Rev.* **2019**, *119*, 4717; d) L. Grill, S. Hecht, *Nat. Chem.* **2020**, *12*, 115.

[2] a) Y.-Q. Zhang, N. Kepčija, M. Kleinschrodt, K. Diller, S. Fischer, A. C. Papageorgiou, F. Allegretti, J. Björk, S. Klyatskaya, F. Klappenberger, M. Ruben, J. V. Barth, *Nat. Commun.* **2012**, *3*, 1286; b) H. Y. Gao, H. Wagner, D. Y. Zhong, J. H. Franke, A. Studer, H. Fuchs, *Angew. Chem., Int. Ed.* **2013**, *52*, 4024; c) J. Liu, P. Ruffieux, X. L. Feng, K. Müllen, R. Fasel, *Chem. Commun.* **2014**, *50*, 11200; d) J. Eichhorn, W. M. Heckl, M. Lackinger, *Chem. Commun.* **2013**, *49*, 2900.

[3] a) F. Diederich, *Nature* **1994**, *369*, 199; b) R. H. Baughman, H. Eckhardt, M. Kertesz, *J. Chem. Phys.* **1987**, *87*, 6687; c) M. M. Haley, S. C. Brand, J. J. Pak, *Angew. Chem., Int. Ed.* **1997**, *36*, 836; d) A. Hirsch, *Nat. Mater.* **2010**, *9*, 868.

[4] a) F. Klappenberger, Y.-Q. Zhang, J. Björk, S. Klyatskaya, M. Ruben, J. V. Barth, *Acc. Chem. Res.* **2015**, *48*, 2140; b) X. Li, H. Zhang, L. Chi, *Adv. Mater.* **2019**, *31*, 1804087.

[5] X. Li, K. Niu, S. Duan, Y. Tang, Z. Hao, Z. Xu, H. Ge, J. Rosen, J. Björk, H. Zhang, X. Xu, L. Chi, *J. Am. Chem. Soc.* **2023**, *145*, 4545.

[6] a) V. K. Kanuru, G. Kyriakou, S. K. Beaumont, A. C. Papageorgiou, D. J. Watson, R. M. Lambert, *J. Am. Chem. Soc.* **2010**, *132*, 8081; b) C. Sanchez-Sanchez, N. Orozco, J. P. Holgado, S. K. Beaumont, G. Kyriakou, D. J. Watson, A. R. Gonzalez-Elipe, L. Feria, J. Fernandez Sanz, R. M. Lambert, *J. Am. Chem. Soc.* **2015**, *137*, 940; c) R. Zhang, G. Lyu, D. Y. Li, P. N. Liu, N. Lin, *Chem. Commun.* **2017**, *53*, 1731.

[7] a) H. Zhou, J. Liu, S. Du, L. Zhang, G. Li, Y. Zhang, B. Z. Tang, H.-J. Gao, *J. Am. Chem. Soc.* **2014**, *136*, 5567; b) T. Lin, L. Zhang, J. Björk, Z. Chen, M. Ruben, J. V. Barth, F. Klappenberger, *Chem.-Eur. J.* **2017**, *23*, 15588.

[8] a) O. Díaz Arado, H. Mönig, H. Wagner, J.-H. Franke, G. Langewisch, P. A. Held, A. Studer, H. Fuchs, *ACS Nano* **2013**, *7*, 8509; b) F. Bebensee, C. Bombis, S. R. Vadapoo, J. R. Cramer, F. Besenbacher, K. V. Gothelf, T. R. Linderoth, *J. Am. Chem. Soc.* **2013**, *135*, 2136.

[9] a) A. Riss, S. Wickenburg, P. Gorman, L. Z. Tan, H.-Z. Tsai, D. G. de Oteyza, Y.-C. Chen, A. J. Bradley, M. M. Ugeda, G. Etkin, S. G. Louie, F. R. Fischer, M. F. Crommie, *Nano Lett.* **2014**, *14*, 2251; b) A. Riss, A. P. Paz, S. Wickenburg, H. Z. Tsai, D. G. De Oteyza, A. J. Bradley, M. M. Ugeda, P. Gorman, H. S. Jung, M. F. Crommie, A. Rubio, F. R. Fischer, *Nat. Chem.* **2016**, *8*, 678.

[10] a) Y.-Q. Zhang, M. Paszkiewicz, P. Du, L. Zhang, T. Lin, Z. Chen, S. Klyatskaya, M. Ruben, A. P. Seitsonen, J. V. Barth, F. Klappenberger, *Nat. Chem.* **2018**, *10*, 296; b) T. Wang, H. Lv, L. Feng, Z. Tao, J. Huang, Q. Fan, X. Wu, J. Zhu, *J. Phys. Chem. C* **2018**, *122*, 14537; c) L. Xing, J. Li, Y. Bai, Y. Lin, L. Xiao, C. Li, D. Zhao, Y. Wang, Q. Chen, J. Liu, K. Wu, *Nat. Commun.* **2024**, *15*, 666.

[11] a) T. Paintner, J. Björk, P. Du, S. Klyatskaya, M. Paszkiewicz, R. Hellwig, M. Uphoff, M. A. Öner, E. Cuniberto, P. S. Deimel, Y.-Q. Zhang, C.-A. Palma, F. Allegretti, M. Ruben, J. V. Barth, F. Klappenberger, *Angew. Chem., Int. Ed.* **2019**, *58*, 11285; b) Y.-Q. Zhang, T. Paintner, R. Hellwig, F. Haag, F. Allegretti, P. Feulner, S. Klyatskaya, M. Ruben, A. P. Seitsonen, J. V. Barth, F. Klappenberger, *J. Am. Chem. Soc.* **2019**, *141*, 5087; c) N. Cao, B. Yang, A. Riss, J. Rosen, J. Björk, J. V. Barth, *Nat. Commun.* **2023**, *14*, 1255.

[12] a) M. S. G. Mohammed, L. Colazzo, A. Gallardo, J. A. Pomposo, P. Jelínek, D. G. de Oteyza, *Chem. Commun.* **2020**, *56*, 8659; b) J. Lawrence, M. S. G. Mohammed, D. Rey, F. Aguilar-Galindo, A. Berdonces-Layunta, D. Peña, D. G. de Oteyza, *ACS Nano* **2021**, *15*, 4937; c) C. Zhang, R. B. Jaculbia, Y. Tanaka, E. Kazuma, H. Imada, N. Hayazawa, A. Muranaka, M. Uchiyama, Y. Kim, *J. Am. Chem. Soc.* **2021**, *143*, 9461.

[13] a) C. Glaser, *Ber. Dtsch. Chem. Ges.* **1896**, *2*, 422; b) A. S. Hay, *J. Org. Chem.* **1962**, *27*, 3320; c) J. Björk, Y.-Q. Zhang, F. Klappenberger, J. V. Barth, S. Stafström, *J. Phys. Chem. C* **2014**, *118*, 3181.

[14] a) L. Gross, F. Mohn, N. Moll, P. Liljeroth, G. Meyer, *Science* **2009**, *325*, 1110; b) L. Gross, B. Schuler, N. Pavliček, S. Fatayer, Z. Majzik, N. Moll, D. Peña, G. Meyer, *Angew. Chem., Int. Ed.* **2018**, *57*, 3888; c) J. Pavel, *J. Phys.: Condens. Matter* **2017**, *29*, 343002.

[15] a) F. J. Giessibl, *Rev. Mod. Phys.* **2003**, *75*, 949; b) F. J. Giessibl, *Rev. Sci. Instrum.* **2019**, *90*, 011101.

[16] N. Kepčija, Y.-Q. Zhang, M. Kleinschrodt, J. Björk, S. Klyatskaya, F. Klappenberger, M. Ruben, J. V. Barth, *J. Phys. Chem. C* **2013**, *117*, 3987.

[17] a) K. Biswas, J. I. Urgel, K. Xu, J. Ma, A. Sánchez-Grande, P. Mutombo, A. Gallardo, K. Lauwaet, B. Mallada, B. de la Torre, A. Matěj, J. M. Gallego, R. Miranda, P. Jelínek, X. Feng, D. Écija, *Angew. Chem., Int. Ed.* **2021**, *60*, 25551; b) M. DeJong, A. J. A. Price, E. Mårsell, G. Tom, G. D. Nguyen, E. R. Johnson, S. A. Burke, *Nat. Commun.* **2022**, *13*, 7407; c) A. Kinikar, X.-Y. Wang, M. Di Giovannantonio, J. I. Urgel, P. Liu, K. Eimre, C. A. Pignedoli, S. Stolz, M. Bommert, S. Mishra, Q. Sun, R. Widmer, Z. Qiu, A. Narita, K. Müllen, P. Ruffieux, R. Fasel, *ACS Nanoscience Au* **2023**, https://doi.org/10.1021/acsnanoscienceau.3c00062

[18] a) L. Gross, F. Mohn, N. Moll, B. Schuler, A. Criado, E. Guitian, D. Pena, A. Gourdon, G. Meyer, *Science* **2012**, *337*, 1326; b) M. Neu, N. Moll, L. Gross, G. Meyer, F. J. Giessibl, J. Repp, *Phys. Rev. B* **2014**, *89*, 205407; c) P. Hapala, G. Kichin, C. Wagner, F. S. Tautz, R. Temirov, P. Jelínek, *Phys. Rev. B* **2014**, *90*, 085421.

[19] a) D. G. de Oteyza, P. Gorman, Y. C. Chen, S. Wickenburg, A. Riss, D. J. Mowbray, G. Etkin, Z. Pedramrazi, H. Z. Tsai, A. Rubio, M. F. Crommie, F. R. Fischer, *Science* **2013**, *340*, 1434; b) A. Sánchez-Grande, B. de la Torre, J. Santos, B. Cirera, K. Lauwaet, T. Chutora, S. Edalatmanesh, P. Mutombo, J. Rosen, R. Zbořil, R. Miranda, J. Björk, P. Jelínek, N. Martín, D. Écija, *Angew. Chem., Int. Ed.* **2019**, *58*, 6559.

[20] N. Moll, B. Schuler, S. Kawai, F. Xu, L. Peng, A. Orita, J. Otera, A. Curioni, M. Neu, J. Repp, G. Meyer, L. Gross, *Nano Lett.* **2014**, *14*, 6127.

[21] a) B. Cirera, Y.-Q. Zhang, S. Klyatskaya, M. Ruben, F. Klappenberger, J. V. Barth, *ChemCatChem* **2013**, *5*, 3281; b) B. Cirera, Y.-Q. Zhang, J. Björk, S. Klyatskaya, Z. Chen, M. Ruben, J. V. Barth, F. Klappenberger, *Nano Lett.* **2014**, *14*, 1891.

[22] C. Bronner, J. Björk, P. Tegeder, *J. Phys. Chem. C* **2015**, *119*, 486.

[23] a) M. Parschau, D. Passerone, K.-H. Rieder, H. J. Hug, K.-H. Ernst, *Angew. Chem., Int. Ed.* **2009**, *48*, 4065; b) H. H. Kong, S. Yang, H. Y. Gao, A. Timmer, J. P. Hill, O. D. Arado, H. Mönig, X. Y. Huang, Q. Tang, Q. M. Ji, W. Liu, H. Fuchs, *J. Am. Chem. Soc.* **2017**, *139*, 3669.

[24] G. Kresse, J. Furthmüller, *Phys. Rev. B* **1996**, *54*, 11169.

[25] P. E. Blöchl, *Phys. Rev. B* **1994**, *50*, 17953.
[26] M. Dion, H. Rydberg, E. Schröder, D. C. Langreth, B. I. Lundqvist, *Phys. Rev. Lett.* **2004**, *92*, 246401.
[27] I. Hamada, *Phys. Rev. B* **2014**, *89*, 121103.
[28] J. Björk, S. Stafstrom, *Chem Phys Chem* **2014**, *15*, 2851.
[29] G. Henkelman, B. Uberuaga, H. Jónsson, *J. Chem. Phys.* **2000**, *113*, 9901.
[30] J. Kästner, P. Sherwood, *J. Chem. Phys.* **2008**, *128*, 014106.
[31] P. Hapala, R. Temirov, F. S. Tautz, P. Jelínek, *Phys. Rev. Lett.* **2014**, *113*, 226101.